A model for overland flow and associated processes within the Hydroinformatics Modelling System

Franz Simons, Tobias Busse, Jingming Hou, Ilhan Özgen and Reinhard Hinkelmann

ABSTRACT

This paper presents a numerical model suitable for a broad range of surface flow problems such as overland flow, wetting and drying processes, varying flow conditions and shock waves. It is based on solution of two-dimensional fully dynamic shallow water equations using a cell-centred finite-volume method. Numerical fluxes are computed with a Harten, Lax and van Leer approximate Riemann solver with a contact wave restored. The scheme is second-order accurate in space, and a total variation diminishing method is used to avoid spurious oscillations in the solution. For extending the model to rainfall-runoff applications, infiltration is considered as a constant runoff coefficient and by the Green–Ampt model. The model is implemented in the Hydroinformatics Modelling System, an object-oriented framework that enables the implementation and simulation of single and multiple processes in different spatial and temporal resolutions, as well as their interactions. The capabilities of the model are shown by comparison with analytical solutions and experimental data of a flash flood and a surface runoff experiment. Finally, a real rainfall-runoff event in a small alpine catchment is investigated. Overall, good agreement of numerical and analytical results, as well as measurements, has been obtained.

Key words | finite-volume method, integrated modelling, object-oriented programming, overland flow, rainfall-runoff simulation, two-dimensional shallow water equations

Franz Simons (corresponding author)
Tobias Busse
Jingming Hou
Ilhan Özgen
Reinhard Hinkelmann
Chair of Water Resources Management and Modeling of Hydrosystems,
Technische Universität Berlin,
sec. TIB1-B14, Gustav-Meyer-Allee 25,
13355 Berlin,
Germany
E-mail: *franz.simons@wahyd.tu-berlin.de*

NOMENCLATURE

A	area of the considered cell (m^2)
C	Chézy coefficient $(\mathrm{s\,m}^{-1/6})$
c	concentration (–)
D	diffusion coefficient $(\mathrm{m}^2\,\mathrm{s}^{-1})$
d	water depth (m)
ε	vegetation drag related coefficient
η	water elevation above datum: $\eta = z_\mathrm{B} + d$ (m)
$\mathbf{f}$	flux vector
g	standard gravity $(9.81\,\mathrm{m\,s}^{-2})$
Γ	boundary of control volume (m)
I	cumulative infiltration (m)
i	infiltration rate $(\mathrm{m\,s}^{-1})$
K	average residence time (s)
k	index of a face of the considered cell
l_k	length of face k (m)
m_c	contaminant source/sink term (s^{-1})
m_w	water source/sink term $(\mathrm{m\,s}^{-1})$
$\mathbf{n}_k$	normal vector pointing outwards of face k
n	Manning coefficient $(\mathrm{s\,m}^{-1/3})$
n	time step index
∇	del operator: $\nabla = \left(\frac{\partial}{\partial x}, \frac{\partial}{\partial y}\right)^T$
ν_t	turbulent kinematic viscosity $(\mathrm{m}^2\,\mathrm{s}^{-1})$
Ψ	runoff coefficient (–)
Q	discharge $(\mathrm{m}^3\,\mathrm{s}^{-1})$
$\mathbf{q}$	vector of conserved flow variables
r	rainfall intensity $(\mathrm{m\,s}^{-1})$
ρ	density of water $(\mathrm{kg\,m}^{-3})$
S	storage (m^3)

doi: 10.2166/hydro.2013.173

$\mathbf{s}$ source vector
t time (s)
Δt time step (s)
u velocity component in x-direction $(\mathrm{m\,s^{-1}})$
v velocity component in y-direction $(\mathrm{m\,s^{-1}})$
$\mathbf{v}$ velocity vector
V_w specific soil water volume (m)
x X coordinate (m)
y Y coordinate (m)
z_B bottom elevation above datum (m)
Ω control volume ($\mathrm{m^2}$)

INTRODUCTION

For studying the development of flood events, of soil erosion and pollutant transport in natural or urban catchment areas, a detailed simulation of the spatially and temporally varying flow field is necessary.

Lumped models provide integral results and do not allow a high-resolution description of the flow processes (e.g. Taskinen & Bruen 2007). Models based on simplifications of the one- or two-dimensional shallow water equations (SWEs), the so-called kinematic and diffusive wave approximations, can be good approximations in specific situations and they are used frequently for runoff simulations (e.g. Gottardi & Venutelli 1993; He *et al.* 2008; Kolditz *et al.* 2008; Sochala *et al.* 2009; Weill *et al.* 2009; Tseng 2010; Mügler *et al.* 2011). However, these models are not able to handle varying flow conditions accurately, which may appear at sudden changes in the topography or at hydraulic jumps (Yeh *et al.* 2011; Costabile *et al.* 2012b). These approximations will provide poor results in cases that belong to the hydraulic flow simulation, like dam break or flood wave simulation. The fully dynamic SWEs have already been used for overland flow simulations (Zhang & Cundy 1989; Esteves *et al.* 2000; Fiedler & Ramirez 2000). The presented models were based on the finite-difference method and showed promising results. In the context of classical shallow water flow simulation, models based on fully dynamic SWEs have significantly developed in the last decade, and, in particular, schemes based on the finite-volume method and approximate Riemann solvers have gained attention because they are able to handle discontinuities in the flow field (e.g. Bradford & Sanders 2002; Liang *et al.* 2004; Yoon & Kang 2004; Creaco *et al.* 2010). In recent publications, very robust schemes that provide accurate results for cases with varying topography and wetting and drying have been presented based on these models (e.g. Liang & Marche 2009; Song *et al.* 2011; Hou *et al.* 2013).

The improvements of the exploration of high-resolution topography data also allow using these sophisticated SWE models for simulating overland flow. Instead of using two different model concepts for the part of runoff generation in the catchment and shallow flow in the river or flood plain, both processes can be simulated together in one model. However, when simulating overland flow, additional problems occur due to the very small water depth. The variation of the bottom topography is of the same order of magnitude as the water depth, so the source/sink terms have significant influence, and the bed shear stress is very large in comparison to other forces, which can cause instabilities (Zhang & Cundy 1989). Recently, Simpson & Castelltort (2006), Caviedes-Voullième *et al.* (2012) and Costabile *et al.* (2012a) presented models suitable for overland flow, based on a first-order approximate Riemann solution.

In this work, we present a model that allows second-order solution of problems such as overland flow, supercritical flow, subcritical flow, transcritical flow, shock-type flow discontinuities and wet–dry interfaces. The model incorporates the solution of two-dimensional fully dynamic SWEs within the framework of the cell-centred finite-volume method. Numerical fluxes are computed with the Harten, Lax and van Leer approximate Riemann solver with the contact wave restored (HLLC). The scheme is second-order accurate in space, and spurious oscillations in the solution are avoided by a sophisticated total variation diminishing (TVD) method (Hou *et al.* 2012). Due to the hydrostatic reconstruction, the scheme provides accurate and well-balanced results on complex topography, even at wet–dry interfaces (Hou *et al.* 2013).

Simulating hydrological processes requires the consideration of more processes than just surface runoff. To obtain the effective rainfall, a runoff generation model is necessary, which at least considers infiltration into the

soil. A broad range of models varying in complexity are used in the literature, ranging from empirical models like the Green–Ampt model (Tayfur *et al.* 1993; Esteves *et al.* 2000; Fiedler & Ramirez 2000) to those based on the two- or even three-dimensional Richards equation (Singh & Murty Bhallamudi 1998; Sochala *et al.* 2009; Weill *et al.* 2009). For the sake of simplicity, in this paper, infiltration is considered by a constant runoff coefficient and by the Green–Ampt model.

In software development, object-oriented design is a widely used technique. The key concepts of encapsulation, inheritance and abstraction allow the development of reusable, easily maintainable and extendible code. Several authors have already shown the advantages of an object-oriented design in the framework of environmental modelling (Wang *et al.* 2005; Elshorbagy & Ormsbee 2006; Kutija & Murray 2007; Kolditz *et al.* 2008). In hydrology, the interaction of different processes is of importance and has to be taken into account. In addition, different physical and numerical model concepts for each process exist. The development of holistic models, which incorporates several of these processes, can be significantly improved by a flexible and extendible modelling framework, which allows fast prototyping and testing of different physical and numerical methods and algorithms. The Hydroinformatics Modelling System (HMS) is a Java-based object-oriented software framework that has been developed at the Chair of Water Resources Management and Modeling of Hydrosystems, Technische Universität Berlin (Busse *et al.* 2012; Simons *et al.* 2012). HMS follows the idea of a component-based system that allows the integrative coupling of different processes. The generalised design enables the implementation and simulation of single and multiple processes in different spatial and temporal resolutions, as well as the interactions with geospatial information databases. The system combines the advantages of approved numerical methods and the flexibility of contemporary software design.

This paper is structured as follows: first the model concepts are presented; then, the numerical methods and the implementation procedure in HMS are described; four examples show the capabilities of the model in simulating complex shallow water and overland flow; and finally, conclusions are given.

GOVERNING EQUATIONS

The physics of most of the relevant processes are expressed by the so-called transport equations that describe the transport of a characteristic variable, e.g. mass, momentum or heat. Although the equations are used for quite different processes, the solution methods are similar. In our work, we took advantage of this fact and developed a software framework that provides general methods to solve problems based on transport equations. The goal is to obtain a flexible framework that provides the possibility to easily implement new processes and to test different numerical methods. The general form of the two-dimensional conservation law can be expressed as:

$$\frac{\partial \mathbf{q}}{\partial t} + \nabla \cdot \mathbf{f} = \mathbf{s} \tag{1}$$

In the following sections, various processes can be regarded in the general form by defining a specific set of the vectors $\mathbf{q}$, $\mathbf{f}$ and $\mathbf{s}$.

Shallow water flow

Using the general conservation law (Equation (1)), the two-dimensional SWEs are written with the vectors:

$$\mathbf{q} = \begin{bmatrix} d \\ ud \\ vd \end{bmatrix}, \quad \mathbf{f} = \begin{bmatrix} \mathbf{v}d \\ \mathbf{v}ud + \frac{1}{2}gd^2\hat{x} - \nu_t \nabla(ud) \\ \mathbf{v}vd + \frac{1}{2}gd^2\hat{y} - \nu_t \nabla(vd) \end{bmatrix},$$
$$\mathbf{s} = \begin{bmatrix} m_w \\ -\frac{\tau_{Bx}}{\rho} - gd\frac{\partial z_B}{\partial x} \\ -\frac{\tau_{By}}{\rho} - gd\frac{\partial z_B}{\partial y} \end{bmatrix} \tag{2}$$

where $\hat{x}$ and $\hat{y}$ are the unit vectors of the cartesian coordinate system given as $\hat{x} = (1, 0)$ and $\hat{y} = (0, 1)$.

The bed friction term can be written as:

$$-\frac{\tau_B}{\rho} = -\frac{g}{C^2}|\mathbf{v}|\mathbf{v} \tag{3}$$

where C can be either a constant value as in the original Chézy law or it can be a function to express, for example,

the Manning law: $C = d^{16}n^{-1}$. The turbulent viscosity ν_t can be either a constant or computed by a turbulence model. In the examples shown in this work, the influence of the turbulence is neglected.

Runoff generation/infiltration model

For the simulation of overland flow on permeable surfaces, the effective rainfall must be known. It is determined by a runoff generation model including infiltration and other processes, e.g. evapotranspiration for long-term simulations. In HMS, two approaches are available to consider the infiltration. The first one is the implementation of simple infiltration models such as the Green–Ampt model (Green & Ampt 1911). The second one is to couple the software with an existing three-dimensional soil model solving the Richards or two-phase flow equations (Notay *et al.* 2012). Using the first approach, the conservation of the specific soil water volume can be expressed as:

$$\mathbf{q} = [V_w],\ \mathbf{f} = [0],\ \mathbf{s} = [i] \tag{4}$$

where the infiltration rate i will be computed by the Green–Ampt model.

Shallow water transport

The transport of a component in shallow water flows can be expressed as:

$$\mathbf{q} = [cd],\ \mathbf{f} = [\mathbf{v}cd - D\nabla(cd)],\ \mathbf{s} = [m_c] \tag{5}$$

As in Equation (2), m is a source/sink term that could be, for example, a reaction process. When simulating multiple-component transport, conservation laws for each component must be formulated.

NUMERICAL METHODS

In this section, the most important details on the numerical methods used in the presented model are described. For further insights, we will refer to other literature.

Time updating

In HMS, the general form of the conservation law (Equation (1)) is discretised with the cell-centred finite-volume method. To update the conserved variables $\mathbf{q}$ in Equation (1) to the new time level, the explicit forward Euler method is chosen:

$$\mathbf{q}^{n+1} = \mathbf{q}^n - \frac{\Delta t}{A}\sum_k \mathbf{f}_k^n \cdot \mathbf{n}_k l_k + \Delta t\, \mathbf{s}^n \tag{6}$$

The time step is determined by the Courant–Friedrichs–Lewy (CFL) criterion to achieve stable results.

Shallow water flow

Interface flux calculation

To calculate the numerical fluxes of mass and momentum (Equation (2)) at the considered face, the HLLC (Toro *et al.* 1994) is used, and the flux $\mathbf{f}_k^n \cdot \mathbf{n}_k$ in Equation (6) can be expressed as:

$$\mathbf{f}_k^n \cdot \mathbf{n}_k = \mathbf{f}_k^n(d_k^L,\ \mathbf{v}_k^L,\ d_k^R,\ \mathbf{v}_k^R,\ \mathbf{n}_k) \tag{7}$$

where L and R denote the left and right Riemann states, respectively. In this work, the left cell is always the one under consideration. For the first-order scheme, the Riemann states are equal to the values at the centre of the left or right cell and in the second-order scheme, the TVD method is used to extrapolate the cell values to the considered face, as shown in Hou *et al.* (2012). The minmod limiter was used in all presented test cases.

Hydrostatic reconstruction

The hydrostatic reconstruction is an efficient and robust approach to preserve non-negative water depths and a well-balanced state in a flow field on varying bottom topography including wet–dry interfaces (Audusse *et al.* 2004; Audusse & Bristeau 2005). The water depth and bottom elevation are modified prior to the Riemann solution

(Hou *et al.* 2013). The bed elevation at the interface k is computed as:

$$z_{Bk} = \max\left(z_B^L, z_B^R\right) \tag{8}$$

Then, the lower value between the bed elevation at k and the water elevation on the left-hand side is chosen as the new bed elevation at face k:

$$z_{Bk} \leftarrow \min\left(z_{Bk}, \eta_k^L\right) \tag{9}$$

Finally, the water depths are reconstructed by:

$$d_k^R = \max\left(0,\ \eta_k^R - z_{Bk}\right) - \max\left(0,\ z_B^R - z_{Bk}\right),\ d_k^L = \eta_k^L - z_{Bk} \tag{10}$$

In overland flow applications, the water depth can be smaller than the variation of the bottom topography, e.g. on inclined terrain (Figure 1(a)). A first-order hydrostatic reconstruction scheme will reduce this problem to piecewise flux computations between wet and artificial dry cells (Figure 1(b)) and, as a consequence, a wrong flow field and hydrograph will be computed (Berthon & Foucher 2012). This failure can be corrected by a second-order scheme. The sketched flow situation will be discretised as a continuous flow problem (Figure 1(c)), and so it is possible to compute flow of thin water on course grids with steep bottom gradients.

Slope source term treatment

To simplify the solution on arbitrary meshes, the bottom slope source term of a cell (Equation (2)) is transformed into fluxes through its faces (Hou *et al.* 2013). The volume integral of the bottom slope source term $\mathbf{s}_b$ can be expressed as the sum of the bottom slope fluxes:

$$\int_\Omega \mathbf{s}_b \, d\Omega = \oint_\Gamma \mathbf{f}_{bk} \cdot \mathbf{n} \, d\Gamma = \sum_k \mathbf{f}_{bk} \cdot \mathbf{n}_k l_k \tag{11}$$

where the bottom slope flux $\mathbf{f}_{bk}$ is equal to:

$$\mathbf{f}_{bk} \cdot \mathbf{n}_k = \begin{bmatrix} 0 \\ -n_{xk} \frac{1}{2} g \left(d_k^L + d_L\right)\left(z_{Bk} - z_{BL}^L\right) \\ -n_{yk} \frac{1}{2} g \left(d_k^L + d_L\right)\left(z_{Bk} - z_B^L\right) \end{bmatrix} \tag{12}$$

Friction source term treatment

As a consequence of the very small water depths, the bottom friction has a notable influence in overland flow applications. To avoid numerical instabilities, a fully implicit discretisation is used for the friction source term. This is achieved by using a splitting point-implicit method described in Bussing & Murman (1988), Yoon & Kang (2004) and Liang & Marche (2009). Writing the equations of momentum (Equations (1) and (2)) in the point-implicit method gives:

$$\frac{\mathbf{q}^{n+1} - \mathbf{q}^n}{\Delta t} = -\frac{1}{A} \sum_k \mathbf{f}_k^n \cdot \mathbf{n}_k l_k + \mathbf{s}_f^{n+1} \tag{13}$$

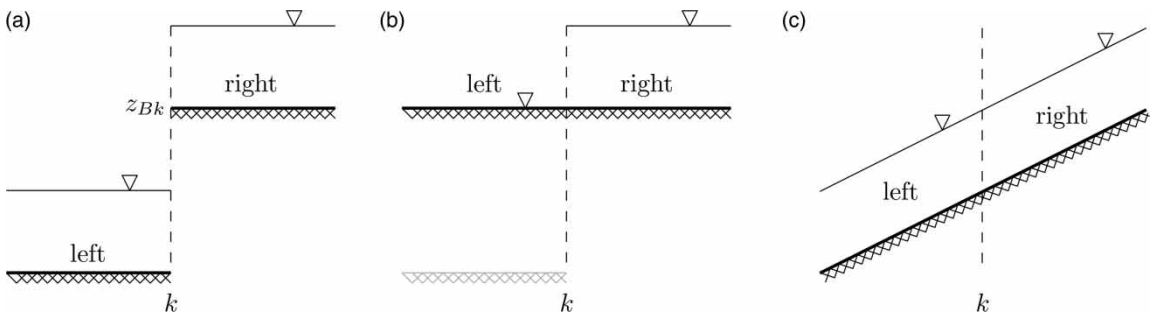

Figure 1 | Influence of hydrostatic reconstruction on the first-order scheme and result of the second-order reconstruction of the face values for water depths smaller than the variation of the bottom topography. (a) Piecewise constant discretisation; (b) Hydrostatic reconstruction with first-order scheme; (c) Hydrostatic reconstruction with second-order scheme.

where $\mathbf{q} = (ud, vd)^{\mathrm{T}}$ in this section. $\mathbf{s}_{\mathrm{f}}^{n+1}$ can be expressed using a Taylor series expansion around the nth time level:

$$\mathbf{s}_{\mathrm{f}}^{n+1} = \mathbf{s}_{\mathrm{f}}^{n} + \left(\frac{\partial \mathbf{s}_{\mathrm{f}}}{\partial \mathbf{q}}\right)^{n} \Delta\mathbf{q} + O(\Delta\mathbf{q}^2) \tag{14}$$

where $\Delta\mathbf{q} = \mathbf{q}^{n+1} - \mathbf{q}^{n}$. Following the procedure given by Bussing & Murman (1988), substituting Equation (14) into Equation (13) yields:

$$\frac{\mathbf{q}^{n+1} - \mathbf{q}^{n}}{\Delta t} = -\frac{1}{A}\sum_{k} \mathbf{f}_{k}^{n} \cdot \mathbf{n}_{k} l_{k} + \mathbf{s}_{\mathrm{f}}^{n} + \left[\left(\frac{\partial \mathbf{s}_{\mathrm{f}}}{\partial \mathbf{q}}\right)^{n} (\mathbf{q}^{n+1} - \mathbf{q}^{n})\right] \tag{15}$$

which can be rewritten as:

$$\mathbf{PI}\left(\frac{\mathbf{q}^{n+1} - \mathbf{q}^{n}}{\Delta t}\right) = -\frac{1}{A}\sum_{k} \mathbf{f}_{k}^{n} \cdot \mathbf{n}_{k} l_{k} + \mathbf{s}_{\mathrm{f}}^{n} \tag{16}$$

where the matrix **PI** is equal to:

$$\mathbf{PI} = \mathbf{I} - \left(\frac{\partial \mathbf{s}_{\mathrm{f}}}{\partial \mathbf{q}}\right)^{n} \tag{17}$$

Herein, **I** is the identity matrix and $(\partial \mathbf{s}_{\mathrm{f}}/\partial \mathbf{q})^{n} = \mathbf{J}_{\mathrm{f}}$ is the Jacobian matrix of the friction source term. During the simulation, the friction and source terms are computed on the old time level, and are then divided by **PI** to get the final solution:

$$\mathbf{q}^{n+1} = \mathbf{q}^{n} + \frac{1}{\mathbf{PI}}\left(-\frac{\Delta t}{A}\sum_{k} \mathbf{f}_{k}^{n} \cdot \mathbf{n}_{k} l_{k} + \Delta t\, \mathbf{s}_{\mathrm{f}}^{n}\right) \tag{18}$$

Runoff generation model

The soil water volume conservation Equation (4) is also solved using the finite-volume method (Equation (6)). As the flux term is equal to zero, it is just necessary to solve the source term that contains the infiltration rate:

$$i = -\frac{I^{n+1} - I^{n}}{\Delta t} \tag{19}$$

where the cumulative infiltration of the new time step, I^{n+1}, is computed by solving the Green–Ampt equation iteratively (Fiedler & Ramirez 2000). Before updating the soil water volume, it is limited to the maximum water volume that is available for infiltration. In addition, a residual rate is computed as an input for the shallow water flow model (Equation (2)) as:

$$m = \frac{V_{\mathrm{w}}^{n+1} - V_{\mathrm{w}}^{n}}{\Delta t} - r \tag{20}$$

where $m < 0$ if the rainfall intensity exceeds the infiltration rate and water is ponding at the surface, and $m > 0$ if the infiltration rate is higher than the rainfall intensity. The model describes so-called infiltration excess or Hortonion runoff (Weill *et al.* 2009).

Shallow water transport

The solution of the transport Equation (5) can be incorporated in the Riemann solver used for solving the SWEs. As transport will not be considered in this paper, no details are given on this here, and the reader is referred to, for example, Heng *et al.* (2009) and Murillo *et al.* (2009).

IMPLEMENTATION IN HMS

Layer concept

In HMS, information is represented in *Layers*. A *Layer* can be a numerical model simulating a certain process, it can be a database storing geospatial data or even some external data sources. Independently, each *Layer* contains geometrical information and data that can be accessed from outside. Via generalised interfaces and data mapping, it is possible to exchange information and to couple *Layers* with each other. Although the *Layer* concept favours one *Layer* for each process, e.g. surface flow, tracer transport or runoff generation, it is not mandatory. Following the idea of one Layer for each process allows a strict splitting of the implementation, which is used to compute the process and the data computed for each process. In addition, it allows the processes to be run independently of each

other. Currently, this concept is followed in the presented model.

Numerical computations

All *Layers* are registered in a *LayerManager* that triggers each *Layer* to perform a certain task and provides a global time loop. *Layers* with time varying data contain an *Engine* that modifies the data of the *Layer*. A numerical-based *Engine* controls the solution of the numerical equations. The *Engine* is triggered by the *LayerManager* to forward the simulation to the next time step.

As already mentioned, the overall time loop is controlled by the *LayerManager*. However, the choice of *Engine* will determine if the governing equations are solved in an explicit or implicit manner to update the solution to the given time level. The advancing in time is divided into three steps: prepare, compute and update. In the context of the finite-volume method, these steps correspond to preparing all variables necessary for the computation, computing all necessary terms and updating the state variables to the new time level. After performing the tasks belonging to one of these steps, the *Engine* waits for the next trigger of the *LayerManager*. This means it is possible to run multiple processes in parallel and exchange data among them.

To separate the *Engine* from the actual physics and numerical methods, the *Engine* solves the general transport equation (Equation (1)) and forwards the task of computing the terms to a so-called *Scheme*. A *Scheme* represents different physical processes, like shallow water flow or transport, and different numerical methods, too. The latter could be, for example, a simple first-order upwind method or the second-order approximate Riemann solution used in this paper to solve the flux term in the SWEs. All numerical algorithms are implemented as abstract and generic as possible, and are included in libraries to make them reusable.

Parallelisation and coupling strategy

To reduce the computational time used for high-resolution case studies or large-scale computations, code parallelisation is useful. The numerical algorithms of HMS are parallelised using the Java thread concept and creating a thread for each available core. This allows efficient computations on shared-memory multicore computers. Because of the explicit time-stepping method used in this paper, a simple procedure can be used for parallelisation: the amount of computational cells is evenly distributed on the threads, and the numerical algorithms are subdivided into parts that can run in parallel. After each part, the threads are waiting for each other before starting the next step. Although this parallelisation technique is pretty straightforward, there is a good scale-up of computational time on desktop and high-performance computers. Even though the numerical algorithm can run in parallel, the execution of the *Layers* or *Engines* is still sequential. To couple different *Layers* or processes, each conservation law is solved sequentially, and data are exchanged after every time step. All processes implemented so far allow weak coupling, i.e. while computing the new time step, a process is independent of the others. In addition, it is possible to couple HMS with external models via generalised interfaces (Notay *et al.* 2012).

EXAMPLES

In the following four examples, the capabilities of the model are presented. Further benchmarks and examples can be found in Simons *et al.* (2012) and Hou *et al.* (2013).

Flash flood in a simplified urban district

In this example, simulation results are compared to experimental data of a test case that includes varying bottom topography, wetting and drying, and complex flow conditions. As part of the joint European project Investigation of Extreme Flood Processes & Uncertainty (IMPACT), Testa *et al.* (2007) acquired experimental data for a test case of a flash flood in a simplified urban district. The domain of consideration is a 1:100 scaled physical model of the Toce River valley. The topography data were obtained by measurements of the model with a spacing of 0.05 m. The model city in the considered domain consists of 20 houses with the positions shown in Figure 2(a). The complete setup of the experiment can be found in Testa *et al.* (2007). On the upstream, an inflow boundary condition computed

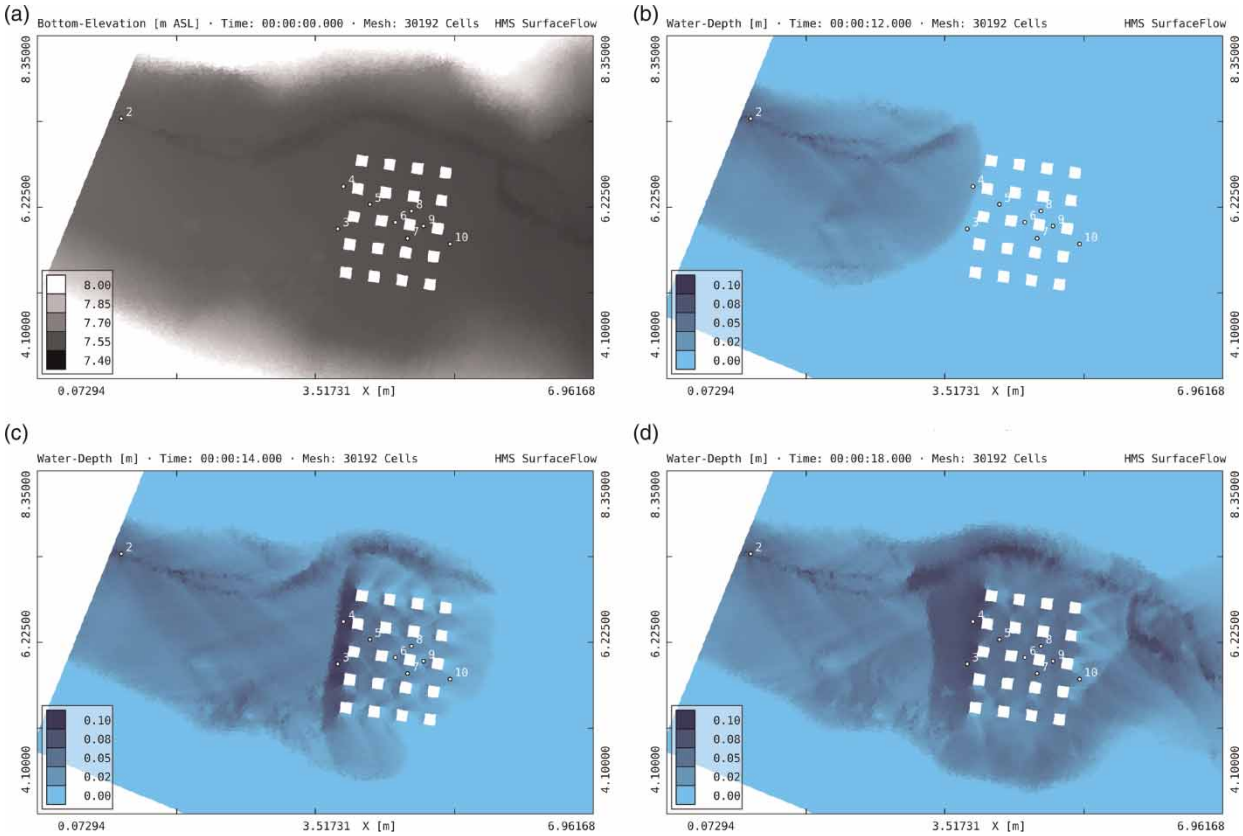

Figure 2 | Domain topography, positions of gauges and simulated flood propagation for the flash flood experiment (m). (a) Domain topography; (b) $t = 12$ s; (c) $t = 14$ s; (d) $t = 18$ s.

from the measured discharge into the feeding tank is imposed. Downstream, a non-reflective outflow boundary condition is chosen. All other boundaries are closed. The experimental data are obtained through ten electrical conductivity gauges placed on different spots in the domain under consideration, measuring 0.2 s. The location of the considered gauges is shown in Figure 2(a). The data used for this boundary condition are denoted as case 'Low' in Testa *et al.* (2007), which refers to a low peak inflow. The initial water depth is set to 0.0 m over the whole domain. Friction is calculated with a Manning coefficient $n = 0.0162\ \mathrm{s\,m^{-1/3}}$ (Testa *et al.* 2007), and turbulence is neglected. The domain is discretised with a total amount of 30,192 triangular cells with an average size of 0.05 m. The time step is calculated adaptively with a CFL number of 0.5.

The simulated flood propagations after 12, 14 and 18 s are plotted in Figures 2(b), 2(c) and 2(d), respectively. In Figure 3, the measured water depths at gauges 2–10 are compared to the numerical results. A relative error is computed from the deviation of the observed and simulated values normalised by the average value:

$$\text{Relative error} = \frac{\sum_i^N \left| \mathbf{q}_{i,\text{obs}} - \mathbf{q}_{i,\text{sim}} \right|}{\sum_i^N \mathbf{q}_{i,\text{obs}}} \times 100\ (\%) \tag{21}$$

where the subscripts obs and sim denote the observed and simulated values, respectively, and N is the total number of observations. The results for the simulated water depths are given in Table 1. Overall, the simulation shows good agreement with the measurements, with a relative error between 7.3 and 22.7%. The arrival time of the wave is simulated correctly. The largest deviation can be observed at gauge 5 (Figure 3(d)), with a maximum of 0.02 m and a relative error of 51.6%. A similar deviation can also be found in Sanders *et al.* (2008) and Soares-Frazão *et al.* (2008).

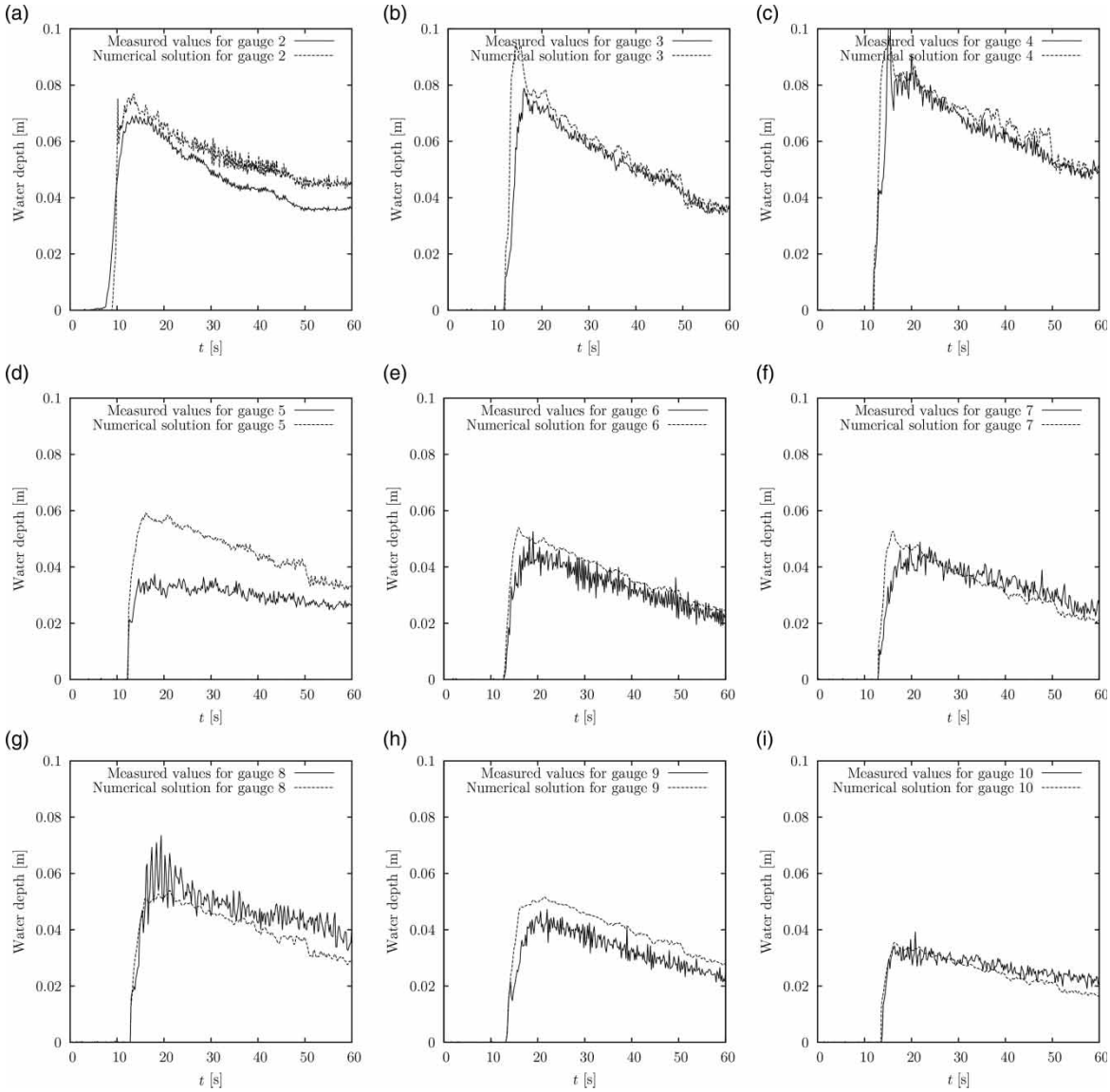

Figure 3 | Comparison of numerical and experimental results of the water depth at gauges 2–10. (a) Gauge 2; (b) Gauge 3; (c) Gauge 4; (d) Gauge 5; (e) Gauge 6; (f) Gauge 7; (g) Gauge 8; (h) Gauge 9; (i) Gauge 10.

V-shaped schematic catchment

This test case aims to show the accuracy of the presented model in simulating shallow surface runoff, and it allows comparison of the first- and second-order scheme. Overton & Brakensiek (1970) presented an approximated kinematic solution of the hydrograph for a long steady and uniform rain event for a V-shaped schematic catchment. The geometry is given in Figure 4, where all parameters used in this simulation are taken from Di Giammarco *et al.* (1996). The slope of the catchment is 0.05, and the channel slope is 0.02. The channel has a width of 20 m and the depth varies from 1 m at the upstream end to 20 m at the downstream end. The Manning roughness coefficients are $0.015\ \mathrm{s\,m^{-1/3}}$ for the hillsides and $0.015\ \mathrm{s\,m^{-1/3}}$ for the channel. The domain was discretised by a uniform rectangular mesh with a cell size of 10 m. All boundaries beside the channel flow are closed boundaries, except the outlet, where

Table 1 | Relative errors of the simulated water depth at gauges 2–10

Gauge	Relative error (%)
2	16.8
3	9.4
4	7.3
5	51.6
6	15.0
7	12.6
8	14.3
9	22.7
10	11.1

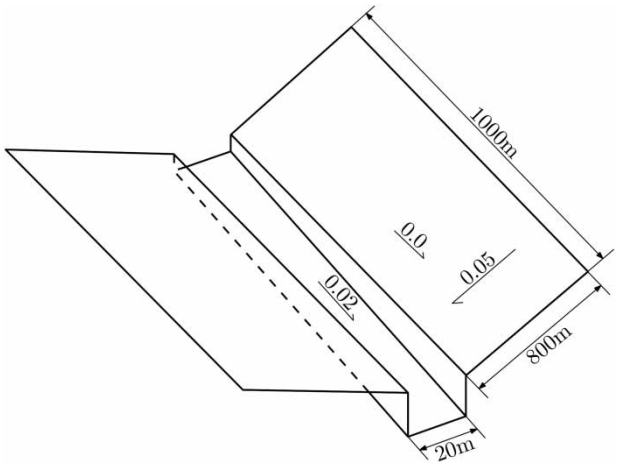

Figure 4 | Geometry of the V-shaped schematic catchment.

critical flow depth was assumed. The CFL criterion was set to 0.1. A constant rainfall with an intensity of 10.8 mm h^{-1} and a duration of 1.5 h was imposed on the hillsides.

In Figure 5, the numerical results of the first- and second-order scheme are compared with the analytical solution (Overton & Brakensiek 1970; Stephenson & Meadows 1986) at the lower end of one hillside and at the outlet of the domain. There is no analytical solution for the descending phase of the discharge at the channel outlet. The relative errors according to Equation (21) are given in Table 2. The results show a very good agreement of the second-order scheme with the analytical solution. For the first-order scheme, the results for the ascending and descending phase are poor, and strong detention can be recognised. As mentioned previously, this can be explained by the very small water depth in the catchment, which is below the variation of the bottom topography in a cell.

Surface runoff experiment

This example is about a rainfall simulation experiment that was carried out in Thies, Senegal, and was presented by Tatard *et al.* (2008) and Mügler *et al.* (2011). The example was chosen as a benchmark test because not only the total discharge was measured, but also local flow velocities inside the domain at stationary flow conditions. By comparing measured and simulated velocities, it is possible to evaluate the model's ability to compute both accurate flow fields and accurate integral results. Mügler *et al.* (2011)

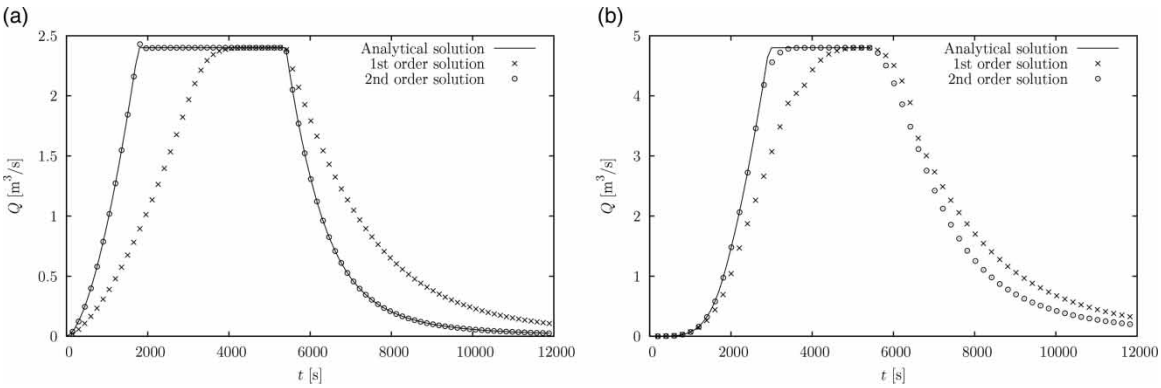

Figure 5 | Comparison of analytical and numerical solution of the first- and second-order scheme. (a) Hydrograph at one hillside; (b) hydrograph at channel outlet.

Table 2 | Relative errors for first- and second-order scheme (%)

	1st order	2nd order
Hydrograph at one hillside	34.5	0.1
Hydrograph at channel outlet	14.5	0.7

presented results for steady-state conditions only; however, Weill (2007) used a fully coupled model based on the diffusive wave approximation and Richard's equation on the entire hydrograph. In this section, we will first present the results of the steady-state case to show the accuracy of the presented model by comparing its results with measured flow velocities. We then present instationary results for the entire hydrograph using the Green–Ampt infiltration model.

The rainfall simulation plot was 10 m long and 4 m wide, with a 1% slope and sandy soil. The plot preparation is described in detail by Mügler *et al.* (2011). The domain topography is given by a $0.1\,\mathrm{m} \times 0.1\,\mathrm{m}$ digital elevation model (Figure 6). For the numerical simulation, the domain was discretised by a uniform rectangular mesh with 4,141 cells. The upstream boundary condition was set as outflow; all other boundaries were set as closed. The water depth-dependent friction formulation of Jain *et al.* (2004) was implemented. Using this approach, the Chézy coefficient in Equation (3) is expressed as:

$$C = d^{1/6} n_0^{-1} \left(\frac{d}{d_0}\right)^{\varepsilon} \tag{22}$$

where n_0 is the minimum land surface-dependent Manning roughness corresponding to flow depth d_0, beyond which n is assumed to be constant, and ε is a coefficient related to vegetation drag (Jain *et al.* 2004).

For the steady-state simulation, infiltration was assumed as constant and, corresponding to the steady-state discharge, an effective rainfall of $51.5\,\mathrm{mm\,h^{-1}}$ was applied. The simulated flow field was compared with mean local flow velocities at 62 points within the entire plot. Due to missing information on the friction properties, the parameters n_0, d_0 and ε were calibrated by minimising the root mean square error (RMSE) of simulated and measured flow velocities. A minimum RMSE of $2.55 \times 10^{-2}\,\mathrm{m\,s^{-1}}$ was obtained by the parameters $n_0 = 0.014\,\mathrm{s\,m^{-13}}$, $d_0 = 0.0045\,\mathrm{m}$ and $\varepsilon = 0.1$. Figure 7 shows the water depth and flow velocity at steady state and the locations of the measurements. In Figure 8, the simulated and measured flow velocities are compared. An overall good agreement can be seen.

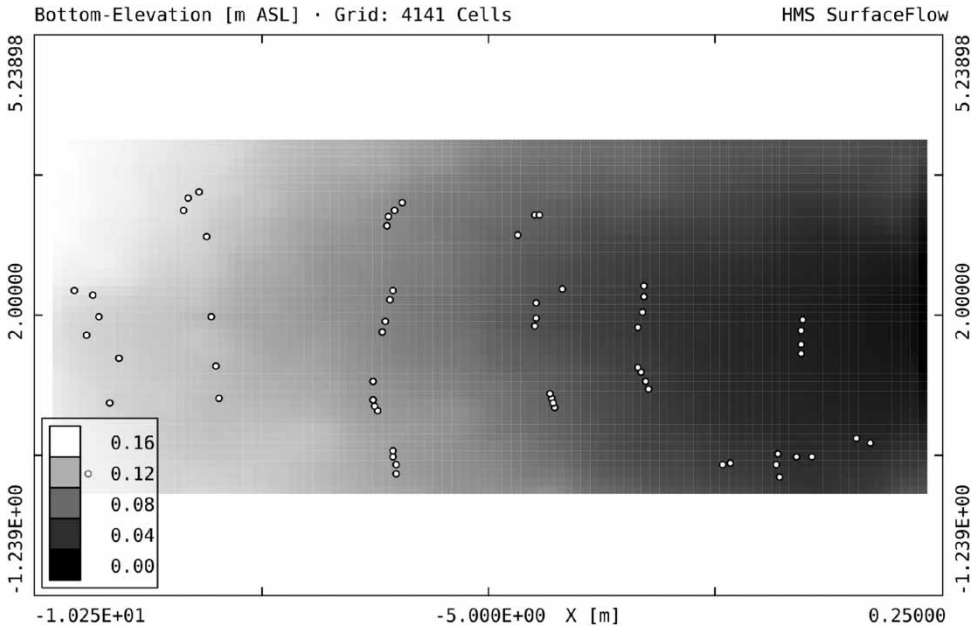

Figure 6 | Domain topography and positions of velocity measurements for the surface runoff experiment (m).

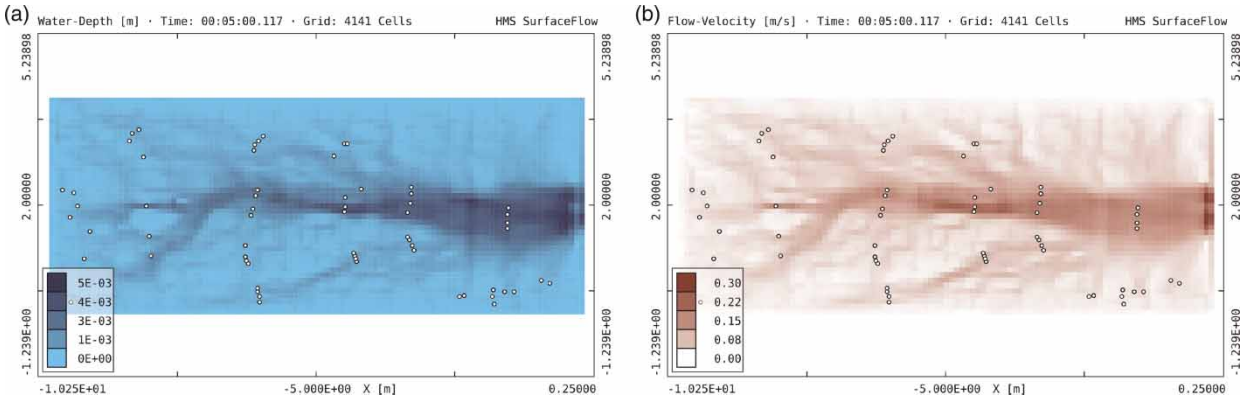

Figure 7 | Simulated water depth (m) and velocity (m s^{-1}) at steady state for the surface runoff experiment. (a) Simulated water depth; (b) simulated flow velocity.

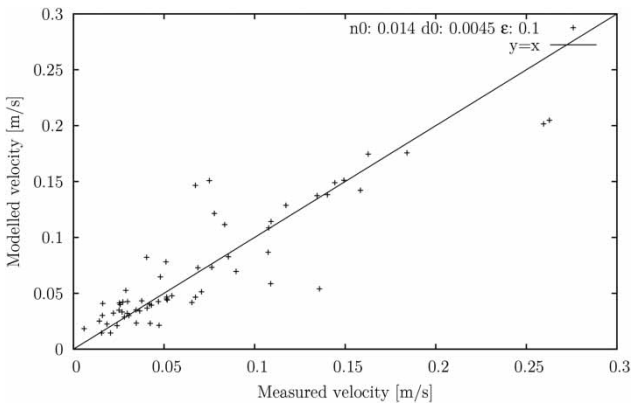

Figure 8 | Simulated versus measured flow velocities with RMSE = 2.55×10^{-2} m s^{-1}.

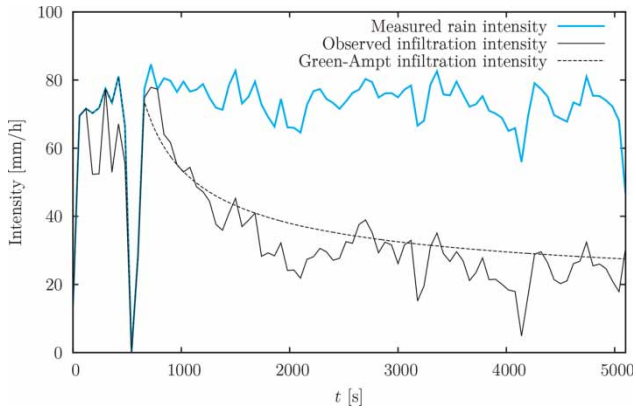

Figure 9 | Comparison of observed and simulated infiltration intensity.

In the second part, an instationary simulation for the entire hydrograph was carried out. During the experiment, the rainfall intensity and the total discharge were recorded. For the simulation, a rainfall time series with a duration of 5,100 s was used as input. The parameters of the Green–Ampt model were approximated by the soil type and calibrated from the steady-state infiltration and the total discharge. In Figure 9, the simulated infiltration intensity is compared with the observed intensity, which was obtained by calculating the difference between measured rain intensity and total runoff. A qualitative agreement can be recognised. The relative error according to Equation (21) for the infiltration intensity is 17.6%. Figure 10 shows a comparison of the measured and simulated total discharge at the outlet of the domain. The overall trend is reproduced

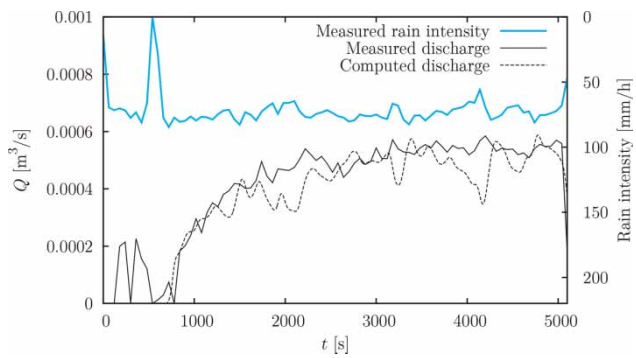

Figure 10 | Comparison of measured and simulated hydrographs.

quite well, with a relative error of 13.7%. However, the measured discharge at the beginning of the event is not captured. Possible explanations are surface coating effects, which are not captured by the Green–Ampt

model. Furthermore, there is no accurate agreement of the simulated and measured discharge at any time. This can also be explained by the simplifications of the Green–Ampt model, which was already shown in Figure 9. The presented model can accurately simulate the surface runoff process that could be shown in the steady-state simulations. However, the runoff generation is, of course, a crucial part, and should be improved in the future.

Small alpine catchment area

The aim of the Deutsche Forschungsgemeinschaft Research Unit 'Coupling of flow and deformation processes for modelling the movement of natural slopes' was to understand and predict the failure of natural slopes. Rainfall, surface runoff and infiltration are possible triggers for landslides, and have been investigated in this project. The study area Heumöser is located in the Vorarlberg Alps (Austria), 10 km south-east of the city of Dornbirn. Further information on the project can be found in Lindenmaier (2008), Wienhöfer *et al.* (2009) and Stadler *et al.* (2012). In this case study, the surface runoff in the subcatchment area of creek 3 with an area of ~100,000 m² (Figure 11, dashed outline) was simulated for a rain event in July 2008 (Simons *et al.* 2011). The bottom elevation was defined by a digital elevation model provided by the 'Wildbach- und Lawinenverbauung', Austria, with a resolution of $1\,\mathrm{m} \times 1\,\mathrm{m}$. All simulations were carried out on a 1 m² uniform rectangular mesh with 147,400 cells. In our investigations, we considered infiltration by a constant runoff coefficient, i.e. a constant amount was subtracted from the measured rainfall.

First, the influences of the friction and the runoff coefficient were studied. For the friction, a small sensitivity was observed. In Figure 12(a), a comparison of measured and simulated discharges for two different runoff coefficients Ψ and a Manning coefficient of $0.067\,\mathrm{s\,m^{-1/3}}$ is given. The results only show qualitative agreement and very high relative errors of 78.0% for $\Psi = 0.3$ and 64.7% for $\Psi = 0.6$ are computed. The poor agreement can be explained by the fact that the surface runoff model does not take into account any slower discharge component in the subsurface such as interflow or groundwater flow. As the focus of this paper is on overland flow, a simple linear reservoir model was added to account for an interflow component. It is described by the continuity equation for the reservoir:

$$\frac{\mathrm{d}S(t)}{\mathrm{d}t} = I(t) - Q(t) \tag{23}$$

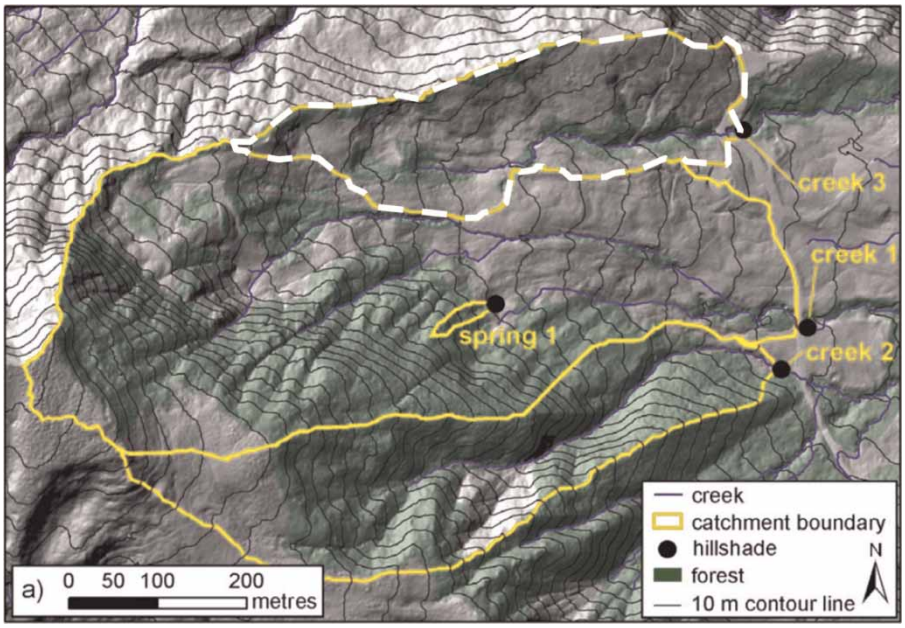

Figure 11 | Subcatchment boundaries at the Heumöser slope (Lindenmaier 2008).

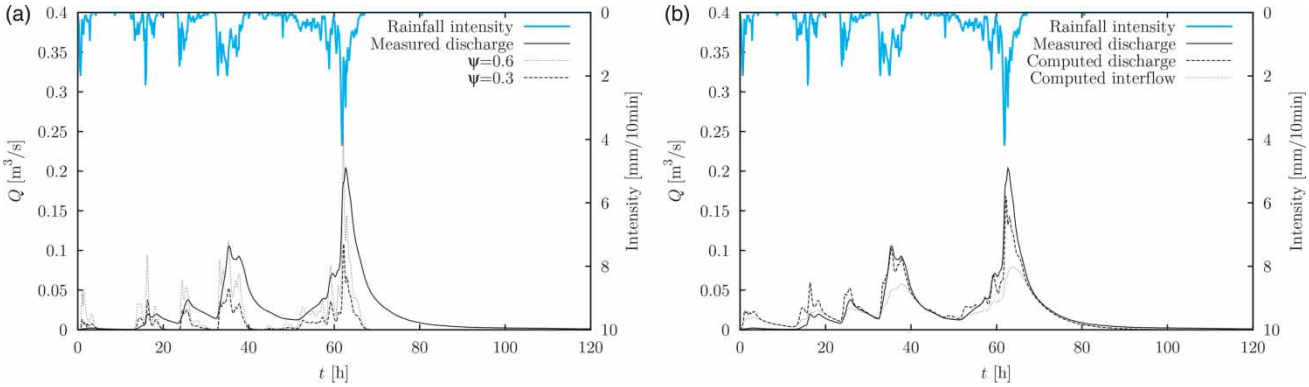

Figure 12 | Simulated hydrographs of the subcatchment 'creek 3'. (a) Comparison of different runoff coefficients; (b) consideration of interflow via linear reservoir model.

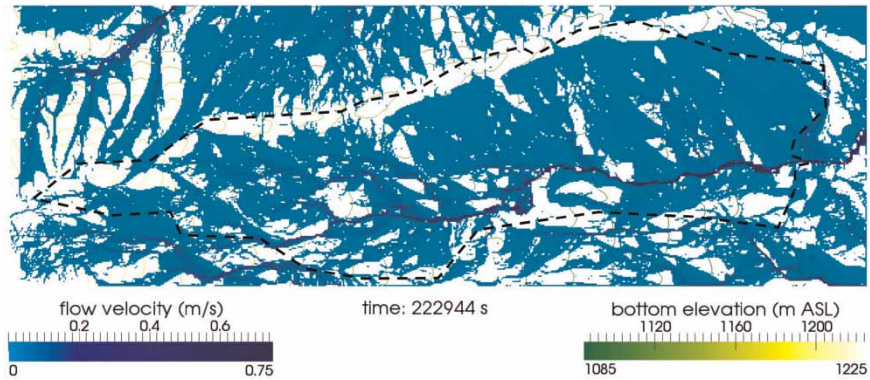

Figure 13 | Simulated flow field at $t = 62$ h.

and a storage–discharge relation:

$$S(t) = K\,Q(t) \tag{24}$$

where $S(t)$ is the storage at time t, $I(t)$ is the inflow and $Q(t)$ is the outflow of the reservoir (e.g. Duggal & Soni 1996). The constant of proportionality K is the average residence time, and is obtained by calibration. The infiltrated amount of water that is determined by the runoff coefficient is used as inflow, and the computed outflow is superimposed with the surface runoff to obtain the total discharge of the domain. For the runoff coefficient $\Psi = 0.3$, an average residence time of $K = 6$ h leads to the best agreement of computed and measured discharges and a relative error of 26.5%, as shown in Figure 12(b). Figure 13 presents the flow field in the domain at $t = 62$ h when the highest discharge was measured for a water depth bigger than 1 mm. Small creeks with high flow velocities (>0.6 m s^{-1}, dark colour) have developed in the domain, while the flow velocities on the surrounding surfaces are below 0.1 m s^{-1} (light colour).

CONCLUSIONS

A two-dimensional model for overland flow and associated processes such as infiltration is presented within the framework of the HMS. It is based on the fully dynamic SWEs and uses the HLLC approximate Riemann solver for flux computation. The scheme is second-order accurate in space, and a TVD scheme is used to avoid spurious oscillations in the solution. Due to the hydrostatic

reconstruction and the splitting point-implicit method to solve the friction term, the model can handle varying bottom topography including wetting and drying and very shallow water depth as they occur in overland flow.

HMS is a Java-based object-oriented software framework which was developed at the Chair of Water Resources Management and Modeling of Hydrosystems, Technische Universität Berlin. It provides a flexible software structure and allows easy implementation of new models, numerical algorithms and coupled processes. In this work, the layer-based approach of HMS is explained and includes details on the implementation. It becomes apparent that HMS supports the development of holistic models that incorporate several processes and their interactions in the context of hydro- and environmental science and engineering.

The model's capabilities were verified against four examples. The first one is the simulation of a flash flood experiment. It shows that the presented model is able to handle strong discontinuities, varying bottom and wetting and drying processes accurately and robustly. In the second example, the model was verified by an idealised analytical test case. Despite very small water depths lower than the variation of the bottom topography, the model showed very good agreement with the analytical solution. The third test case was chosen to show the model's ability not only to produce accurate integral results, but also to compute an accurate flow field. Simulated stationary local flow velocities of an artificial surface runoff experiment were compared with the measurements, and a good agreement was achieved. In the same example, an instationary simulation was carried out, and infiltration was taken into account by the Green–Ampt model. The overall trend of the hydrograph was reproduced quite well. However, further improvements are required concerning the infiltration approximation. In the last example, a simulation of a real rainfall event in a small alpine catchment was investigated. Infiltration was considered by a constant runoff coefficient. It was necessary to add an interflow component in the form of a linear reservoir model to obtain good agreement of the simulated and measured hydrograph.

To summarise, the model is robust and accurate in simulating a broad range of complex shallow water flow problems including overland flow with wetting and drying over complex topography.

ACKNOWLEDGEMENTS

The work on the small alpine catchment area was partly funded by the Deutsche Forschungsgemeinschaft (DFG) in the framework of the research unit 'Coupling of Flow and Deformation Processes for Modeling the Movement of Natural Slopes'. We would also like to thank C. Mügler and O. Planchon for providing the experimental data and additional help for the surface runoff experiment.

REFERENCES

Audusse, E. & Bristeau, M.-O. 2005 A well-balanced positivity preserving 'second-order' scheme for shallow water flows on unstructured meshes. *Journal of Computational Physics* **206** (1), 311–333.

Audusse, E., Bouchut, F., Bristeau, M.-O., Klein, R. & Perthame, B. 2004 A fast and stable well-balanced scheme with hydrostatic reconstruction for shallow water flows. *SIAM Journal on Scientific Computing* **25** (6), 2050–2065.

Berthon, C. & Foucher, F. 2012 Efficient well-balanced hydrostatic upwind schemes for shallow-water equations. *Journal of Computational Physics* **231** (15), 4993–5015.

Bradford, S. F. & Sanders, B. F. 2002 Finite-volume model for shallow-water flooding of arbitrary topography. *Journal of Hydraulic Engineering* **128** (3), 289–298.

Busse, T., Simons, F., Mieth, S., Hinkelmann, R. & Molkenthin, F. 2012 HMS: a generalised software design to enhance the modelling of geospatial referenced flow and transport phenomena. In: *Proc. 10th International Conference on Hydroinformatics.* Hamburg, Germany.

Bussing, T. R. A. & Murman, E. M. 1988 Finite-volume method for the calculation of compressible chemically reacting flows. *AIAA Journal* **26** (9), 1070–1078.

Caviedes-Voullième, D., García-Navarro, P. & Murillo, J. 2012 Influence of mesh structure on 2D full shallow water equations and SCS Curve Number simulation of rainfall/runoff events. *Journal of Hydrology* **448–449**, 39–59.

Costabile, P., Costanzo, C. & Macchione, F. 2012a A storm event watershed model for surface runoff based on 2D fully dynamic wave equations. *Hydrological Processes* **27** (4), 554–569.

Costabile, P., Costanzo, C. & Macchione, F. 2012b Comparative analysis of overland flow models using finite volume schemes. *Journal of Hydroinformatics* **14** (1), 122–135.

Creaco, E., Campisano, A., Khe, A., Modica, C. & Russo, G. 2010 Head reconstruction method to balance flux and source terms in shallow water equations. *Journal of Engineering Mechanics* **136** (4), 517–523.

Di Giammarco, P., Todini, E. & Lamberti, P. 1996 A conservative finite elements approach to overland flow: the control volume finite element formulation. *Journal of Hydrology* **175** (1–4), 267–291.

Duggal, K. N. & Soni, J. P. 1996 *Elements of Water Resources Engineering*, 1st edition. New Age International, New Delhi.

Elshorbagy, A. & Ormsbee, L. 2006 Object-oriented modeling approach to surface water quality management. *Environmental Modelling & Software* **21** (5), 689–698.

Esteves, M., Faucher, X., Galle, S. & Vauclin, M. 2000 Overland flow and infiltration modelling for small plots during unsteady rain: numerical results versus observed values. *Journal of Hydrology* **228** (3–4), 265–282.

Fiedler, F. R. & Ramirez, J. A. 2000 A numerical method for simulating discontinuous shallow flow over an infiltrating surface. *International Journal for Numerical Methods in Fluids* **32** (2), 219–240.

Gottardi, G. & Venutelli, M. 1993 A control-volume finite-element model for two-dimensional overland flow. *Advances in Water Resources* **16** (5), 277–284.

Green, W. H. & Ampt, G. A. 1911 Studies on soil physics, 1, the flow of air and water through soils. *Journal of Agricultural Science* **4** (1), 1–24.

He, Z., Wu, W. & Wang, S. S. Y. 2008 Coupled finite-volume model for 2D surface and 3D subsurface flows. *Journal of Hydrologic Engineering* **13** (9), 835–845.

Heng, B. C. P., Sander, G. C. & Scott, C. F. 2009 Modeling overland flow and soil erosion on nonuniform hillslopes: a finite volume scheme. *Water Resources Research* **45** (5), 1–11.

Hou, J., Liang, Q., Simons, F. & Hinkelmann, R. 2013 A 2D well-balanced shallow flow model for unstructured grids with novel slope source term treatment. *Advances in Water Resources* **52**, 107–131.

Hou, J., Simons, F. & Hinkelmann, R. 2012 Improved total variation diminishing schemes for advection simulation on arbitrary grids. *International Journal for Numerical Methods in Fluids* **70** (3), 359–382.

Jain, M. K., Kothyari, U. C. & Ranga Raju, K. G. 2004 A GIS based distributed rainfall-runoff model. *Journal of Hydrology* **299** (1–2), 107–135.

Kolditz, O., Delfs, J.-O., Bürger, C., Beinhorn, M. & Park, C.-H. 2008 Numerical analysis of coupled hydrosystems based on an object-oriented compartment approach. *Journal of Hydroinformatics* **10** (3), 227–244.

Kutija, V. & Murray, M. G. 2007 An object-oriented approach to the modelling of free-surface flows. *Journal of Hydroinformatics* **9** (2), 81–94.

Liang, Q., Borthwick, A. G. L. & Stelling, G. 2004 Simulation of dam- and dyke-break hydrodynamics on dynamically adaptive quadtree grids. *International Journal for Numerical Methods in Fluids* **46** (2), 127–162.

Liang, Q. & Marche, F. 2009 Numerical resolution of well-balanced shallow water equations with complex source terms. *Advances in Water Resources* **32** (6), 873–884.

Lindenmaier, F. 2008 Hydrology of a Large Unstable Hillslope at Ebnit, Vorarlberg: Identifying Dominating Processes and Structures. PhD Thesis, Universität Potsdam.

Mügler, C., Planchon, O., Patin, J., Weill, S., Silvera, N., Richard, P. & Mouche, E. 2011 Comparison of roughness models to simulate overland flow and tracer transport experiments under simulated rainfall at plot scale. *Journal of Hydrology* **402** (1–2), 25–40.

Murillo, J., García-Navarro, P. & Burguete, J. 2009 Conservative numerical simulation of multi-component transport in two-dimensional unsteady shallow water flow. *Journal of Computational Physics* **228** (15), 5539–5573.

Notay, K. V., Stadler, L., Simons, F., Molkenthin, F. & Hinkelmann, R. 2012 Model coupling in hydroinformatics systems through the use of autonomous tensor objects. In: *Proc. 10th International Conference on Hydroinformatics.* Hamburg, Germany.

Overton, D. & Brakensiek, D. 1970 A kinematic model of surface runoff response. In: *Proc. Wellington Symposium.* Unesco/IAHS, Paris, pp. 100–112.

Sanders, B. F., Schubert, J. E. & Gallegos, H. A. 2008 Integral formulation of shallow-water equations with anisotropic porosity for urban flood modeling. *Journal of Hydrology* **362** (1–2), 19–38.

Simons, F., Busse, T., Hou, J., Notay, K. V. & Hinkelmann, R. 2011 A robust and efficient solver for the shallow water equations and its application to a complex natural hydrosystem. In: *Proc. 34th IAHR Congress.* Engineers Australia, Brisbane, Australia, pp. 4276–4283.

Simons, F., Busse, T., Hou, J., Özgen, I. & Hinkelmann, R. 2012 HMS: model concepts and numerical methods around shallow water flow within an extendable modeling framework. In: *Proc. 10th International Conference on Hydroinformatics.* Hamburg, Germany.

Simpson, G. & Castelltort, S. 2006 Coupled model of surface water flow, sediment transport and morphological evolution. *Computers & Geosciences* **32** (10), 1600–1614.

Singh, V. & Murty Bhallamudi, S. 1998 Conjunctive surface-subsurface modeling of overland flow. *Advances in Water Resources* **21** (7), 567–579.

Soares-Frazão, S., Lhomme, J., Guinot, V. & Zech, Y. 2008 Two-dimensional shallow-water model with porosity for urban flood modelling. *Journal of Hydraulic Research* **46** (1), 45–64.

Sochala, P., Ern, A. & Piperno, S. 2009 Mass conservative BDF-discontinuous Galerkin/explicit finite volume schemes for coupling subsurface and overland flows. *Computer Methods in Applied Mechanics and Engineering* **198** (27–29), 2122–2136.

Song, L., Zhou, J., Li, Q., Yang, X. & Zhang, Y. 2011 An unstructured finite volume model for dam-break floods with wet/dry fronts over complex topography. *International Journal for Numerical Methods in Fluids* **67** (8), 960–980.

Stadler, L., Hinkelmann, R. & Helmig, R. 2012 Modeling macroporous soils with a two-phase dual-permeability model. *Transport in Porous Media* **95**, 585–601.

Stephenson, D. & Meadows, M. E. 1986 *Kinematic Hydrology and Modelling*. Elsevier, Amsterdam.

Taskinen, A. & Bruen, M. 2007 Incremental distributed modelling investigation in a small agricultural catchment: 1. Overland flow with comparison with the unit hydrograph model. *Hydrological Processes* **21** (1), 80–91.

Tatard, L., Planchon, O., Wainwright, J., Nord, G., Favismortlock, D., Silvera, N., Ribolzi, O., Esteves, M. & Huang, C. 2008 Measurement and modelling of high-resolution flow-velocity data under simulated rainfall on a low-slope sandy soil. *Journal of Hydrology* **348** (1–2), 1–12.

Tayfur, G., Kavvas, M. L., Govindaraju, R. S. & Storm, D. E. 1993 Applicability of St. Venant equations for two-dimensional overland flows over rough infiltrating surfaces. *Journal of Hydraulic Engineering* **119** (1), 51–63.

Testa, G., Zuccalà, D., Alcrudo, F., Mulet, J. & Soares-Frazão, S. 2007 Flash flood flow experiment in a simplified urban district. *Journal of Hydraulic Research* **45**, 37–44.

Toro, E. F., Spruce, M. & Speares, W. 1994 Restoration of the contact surface in the HLL-Riemann solver. *Shock Waves* **4** (1), 25–34.

Tseng, M.-H. 2010 Kinematic wave computation using an efficient implicit method. *Journal of Hydroinformatics* **12** (3), 329–338.

Wang, J., Endreny, T. A. & Hassett, J. M. 2005 A flexible modeling package for topographically based watershed hydrology. *Journal of Hydrology* **314** (1–4), 78–91.

Weill, S. 2007 Modélisation des échanges surface/subsurface à l'échelle de la parcelle par une approche darcéenne multidomaine. PhD Thesis, École des Mines de Paris.

Weill, S., Mouche, E. & Patin, J. 2009 A generalized Richards equation for surface/subsurface flow modelling. *Journal of Hydrology* **366** (1–4), 9–20.

Wienhöfer, J., Germer, K., Lindenmaier, F., Färber, A. & Zehe, E. 2009 Applied tracers for the observation of subsurface stormflow at the hillslope scale. *Hydrology and Earth System Sciences* **13** (7), 1145–1161.

Yeh, G.-T., Shih, D.-S. & Cheng, J.-R. C. 2011 An integrated media, integrated processes watershed model. *Computers & Fluids* **45** (1), 2–13.

Yoon, T. H. & Kang, S.-K. 2004 Finite volume model for two-dimensional shallow water flows on unstructured grids. *Journal of Hydraulic Engineering* **130** (7), 678–688.

Zhang, W. & Cundy, T. W. 1989 Modeling of two-dimensional overland flow. *Water Resources Research* **25** (9), 2019–2035.

First received 30 October 2012; accepted in revised form 16 January 2013. Available online 23 February 2013